

Electrochemical and chronoamperometry assessment of nano-gold sensor surfaces produced via novel laser fabrication methods

Cian Hughes, Ronán M. McCann, Brian Freeland, Dermot Brabazon

¹I-Form Advanced Manufacturing Research Centre, Advanced Processing Technology Research Centre, Dublin City University, Glasnevin, Dublin 9, Ireland ^bNational Centre for Sensor Research, Dublin City University, Glasnevin, Dublin 9, Ireland

²School of Mechanical and Manufacturing Engineering, Dublin City University, Dublin, Ireland

Corresponding author: cian.hughes@dcu.ie

Abstract

New developments in laser ablation have shown great potential as nanofabrication methodologies, offering many significant advantages over more traditional methods. Herein, we have developed a method for applying two of these techniques, confined atmospheric pulsed-laser (CAP) deposition and laser ablation synthesis in solution (LASiS), to the fabrication of a nanostructured sensor platform. Following deposition, additional steps were then used to crosslink the deposited nanostructures and fabricate counter and reference electrodes. Chronoamperometry and cyclic voltammetry (CV) were used to assess the effects of these crosslinking steps on the properties of the sensor surfaces. These experiments resulted in the development of a simple, inexpensive and readily scalable process for the fabrication of 3-electrode sensor systems. As an example of a readily measurable surface interaction, electrochemical impedance spectroscopy (EIS) was applied to demonstrate the use of these systems in the detection of 6-mercaptophexanol. This interaction was examined in real-time by measuring the change in the EIS of the sensor system over time following its exposure to the thiol. This experiment clearly showed a measurable EIS response, demonstrating the effectiveness of these newly fabricated sensors for the detection of a simple surface interaction and suggesting the future potential of these laser based methods as the basis for an inexpensive, facile, rapid and scalable sensor fabrication process.

Keywords: Electrochemistry, Sensor, Biosensor, Sensor surface, Nanotechnology, Nanoparticles, Nanostructures, Colloidal nanoparticles, AuNPs, Nanofabrication, Laser deposition, Laser ablation, LASiS, Cap, PLD, Electrochemical impedance spectroscopy, EIS, Chronoamperometry, Sensor fabrication, Novel methods

To cite this article: *Cian Hughes, Ronán M. McCann, Brian Freeland, Dermot Brabazon, Electrochemical and chronoamperometry assessment of nano-gold sensor surfaces produced via novel laser fabrication methods, Journal of Electroanalytical Chemistry, Volume 880, 1 January 2021, 114813.*

1. Introduction

The application of nanotechnology in the design of sensor surfaces has led to a significant increase in their sensitivity in recent times [1,2]. As a result of these benefits, much of the attention in sensor research has been directed towards the exploration of the sensing properties of the various novel and unique types of structures accessible through existing nanofabrication methods [3,4]. Through these explorations it has been found, for example, that porous, layered, nanostructured sensors offer significantly enhanced sensitivity over earlier designs representing a relatively simple path to signal amplification [[5], [6], [7]]. However, these benefits and exciting possibilities for future development have brought with them an increase in both the complexity and cost of biosensor manufacture. The field of nanotechnology as applied to sensor surfaces is still in its relative infancy, leaving many opportunities for future developments in this area. With this in mind, there is a clear need for the research and development of scalable, inexpensive nanofabrication methods to enable sensor designs to reach their application potential [8].

Just as the development of nanostructured sensor platforms has progressed significantly over the past decade so too has the field of nanofabrication. Attempts to apply some of these methodologies to sensor fabrication include strategies such as the development of novel sensing methods [9] or the development of sensors aimed at simpler chemical targets [10] and these efforts have been met with success so far. However, in recent years many novel nanofabrication methodologies have also been developed [[11], [12], [13]] that have not yet been widely applied in sensor preparation. Of these, laser based methods have been of particular interest in nanofabrication research due to their low cost, scalability, high speed and sustainability when compared to more common chemical reduction based methods [14,15]. As such, a logical step pursuant to the goal of designing lower cost, mass producible nanosensors would be to apply these laser nanofabrication techniques to sensor preparation.

For the most part, modern laser surface nanofabrication methodologies that fit these prerequisites can be broadly categorised as either a laser deposition technique or a laser processing in liquids (LPL) technique. Laser deposition techniques such as pulsed laser deposition (PLD) [16,17], laser induced forward transfer (LIFT) [18,19], laser induced reverse transfer (LIRT) [20] and confined atmospheric pulsed-laser (CAP) deposition [21,22] work by ablating a bulk metal and forming an ablation plume which then forms nanostructures on a substrate surface. Similarly, LPL techniques such as laser assisted synthesis in solution also known as pulsed laser ablation in liquid (LASiS / PLAL) [23,24] and pulsed laser melting in liquid (PLML) [25,26] work by irradiating a bulk metal but in these techniques the ejecta plume is expelled into a solvent, where it condenses to form a colloid [14]. As laser based processes, both of these nanofabrication approaches have been shown to offer significant benefits when compared to other nanofabrication techniques being less costly, more applicable to mass production of nanotechnological products, and more green than conventional alternatives [15,27].

Based on these recent advances in nanofabrication, this study focused on the development of an inexpensive, scalable, laser-based methodology for the fabrication of a nanostructured sensor surface. Progressing through 3 successful design stages, the final sensor was gradually converged upon through iterative design by fabricating samples, identifying design flaws,

testing solutions and repeating this process. The final methodology developed makes use of the CAP deposition technique [21] in addition to ‘semi-batch’ LASiS [28] to create a nanostructured gold surface on a polymer substrate, consisting of a matrix of interconnected nanostructures through which electrons can percolate. Several variations on this sensor design were trialled, investigating their effect on the electrochemical response detected. The responsiveness of the generated surfaces was demonstrated in an electrochemical test by examining the binding of a thiol to the sensor surface using Electrochemical Impedance Spectroscopy (EIS). This thiol binding test was used as a benchmarking method, providing a readily detectable surface interaction to measure [29]. The different sensor designs showed clear EIS responses when exposed to a thiol, with the final design exhibiting the most significant change. Thus, the use of this inexpensive and scalable methodology in the fabrication of a functional sensor was assessed.

2. Materials and methods

2.1. Sensor materials and fabrication equipment

The sensors prepared were fabricated using ZeonorFilm ZF14–188 (Zeon Chemical L.P. Japan) Cyclic Olefin Copolymer (COC) as a substrate. All laser processing steps were performed using a 1064 nm Nd:YAG laser with a 140 μm diameter Gaussian profile spot at the focus operated in TEM00 mode. The position of the laser spot during these processes was controlled by a Raylase (DE) SuperScan-12 2-axis galvanometer, while the target position relative to its marking field was controlled using a Physik Instrumente (DE) M-404 precision linear stage. A 10 mm \times 10 mm \times 0.188 mm, 99.9% pure gold metal ablation target was prepared for these laser processing steps from a sputtering target (sourced from Agar Scientific, UK). The target stage (used during CAP deposition) and ablation cell (used during LASiS) were prepared via 3D printing with PlasClear resin on an Asiga (US) Freeform Pico stereolithographic printer and VeroWhite resin with a Stratasys (US) Connex 1 Polyjet respectively.

Screen printing fabrication steps were performed using Ercon (US) E3178 conductive carbon ink on a DEK (US) 248 semi-automatic screen printer. The reagent used during crosslinking sensor fabrication steps was benzene-1,4-dithiol (DTB, 99% GC, Sigma-Aldrich, US). The thiol used for surface interaction tests on finished sensors was 6-mercaptohexanol (97%, Sigma-Aldrich, US). These surface interactions were detected electrochemically using a Gamry (US) Interface 1000E potentiostat. Other conductometric measurements on dry samples were carried out using a BioRad (US) HL5500 4-point Hall effect probe. Solvents used throughout this process included deionised water, ethanol (99%, Sigma-Aldrich, US) and phosphate buffered saline (PBS, tablet, Sigma-Aldrich, US).

2.2. CAP deposition process

Every CAP deposition carried out was performed on COC using a bidirectional raster scan pattern with the target placed at the focal plane of the laser. Depositions were carried out at a scan spacing of 50 μm , scan speed of 18 mm/s, fluence of 0.79 J/cm², a Pulse Repetition Frequency (PRF) of 10 kHz and a pulse width of 3.5 μs . During deposition, the substrate and stage were positioned with a 50 μm gap between them using a 3d printed target stage (Hughes et al., 2018). To carry out the deposition, the gold ablation target was affixed to the stage and the COC substrate was placed above this (Fig. 1 (a)). The laser was then shone through the

substrate (Fig. 1 (b)), ablating the gold and allowing the confined plasma plume to condense into nanostructures on the substrate surface (Fig. 1 (c)).

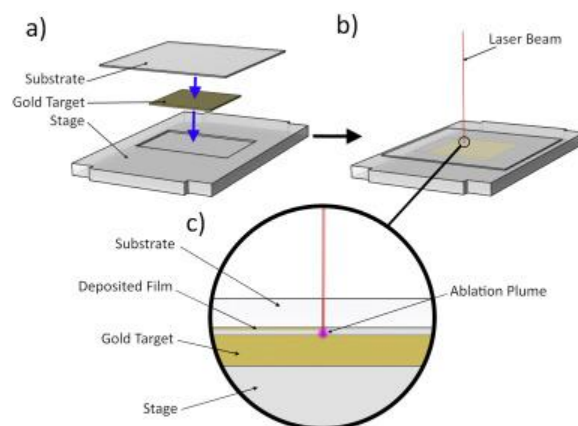


Fig. 1. A schematic of the CAP methodology used during the course of this experiment exhibiting (a) the placement of materials and substrates, (b) the path of the laser during ablation, and (c) an illustration of the deposition process as it occurs.

Various sensor designs were trialed to investigate their effect on the electrochemical response and its sensitivity. The first design (design 1) is presented in Fig. 2 (a). To improve the response of this sensor, the next design developed and tested (design 2) was produced using screen printing to add a conductive, inert carbon contact increasing the measured response. Additionally, the 2d surface area (the surface area of the sensor if we assume a flat topology) was increased between design 1 and 2 from 25 mm² to 100 mm² in an attempt to increase signal. In the final design tested (design 3), the same screen printing method was used to produce counter and reference electrodes, resulting in the creation of a self contained sensor compatible with common “plug & play” testing cell systems. The sensing electrode design dimensions were 5 mm × 5 mm for design 1, 10 mm × 10 mm for design 2, and 5 mm × 5 mm for design 3.

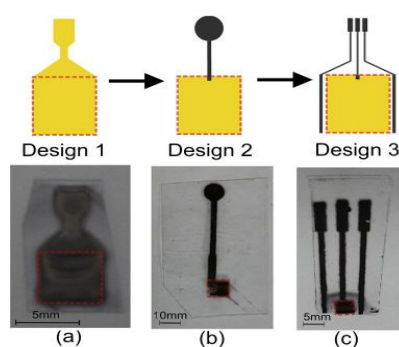


Fig. 2. Schematic illustration of deposited sensor surfaces (outlined with red lines) and electrodes in (a) design 1, (b) design 2, and (c) design 3.

Following deposition, conductive carbon ink was used to screen print a contact in addition to counter and reference electrodes (in the case of design 3) allowing the sensors to be used with common, commercially available 3-electrode electrochemical sensing apparatus. Screen printing was carried out by manually aligning sheets with multiple, properly spaced, CAP

deposited nanostructured squares beneath custom screens allowing for the printing of up to 50 sensors per pass.

2.3. Crosslinking of the sensor surface

Crosslinking of the nanostructured film was then carried out via alternating exposures of the surface to a 0.1% (w/v) solution of DTB in 50:50 water:ethanol solvent and an aqueous 18 nm gold nanoparticle colloid (AuNP colloid). This colloid was produced via continuous flow LASiS [23] over 30 min at a fluence of 1.83 J/cm², a PRF of 10 kHz, a pulse width of 500 ps and a flow rate of 140 mL/min. The nanoparticle size in this colloid was determined using dynamic light scattering (DLS) (Fig. 3). This process proceeded by immersing sensors for 5 min in the DTB solution, followed by 5 min immersion in colloid, followed by another 5 min immersion in DTB and a subsequent return for a further 5 min colloid immersion. Between each immersion, the sensors were rinsed with a small amount of ethanol to minimise cross-contamination of reagents.

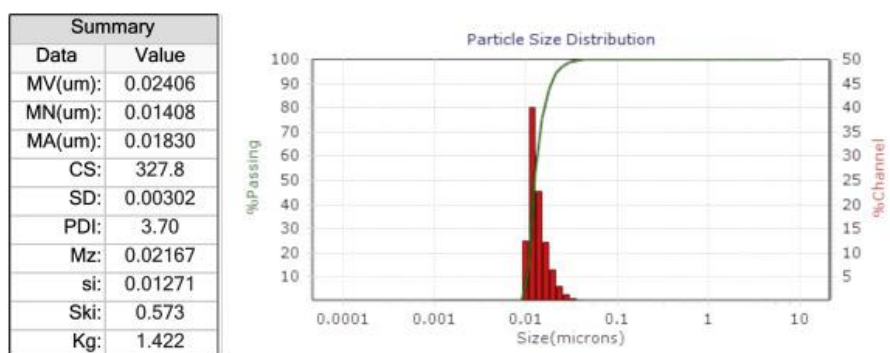


Fig. 3. The DLS scan data for the LASiS produced colloidal gold nanoparticles used during sensor fabrication.

This crosslinking step was performed to enhance the conductivity of the deposited surfaces. By applying this method utilising a molecule such as benzene-1,4-dithiol it was hypothesised that charge could be conveyed between adjacent, non-contacting nanostructures (Fig. 4). By then exposing the surface to colloidal nanoparticles it would be possible to daisy-chain gold nanostructures to bridge any gaps that might be present, while conferring the additional benefit of further increasing the 3d surface area of the film (that being the total surface area of the 3d nanostructures present). Tests found that the resistivity of the films could be successfully reduced from the previously reported value of $>1E+10 \Omega/\text{sheet}$ to a value between $3.9E+4 \Omega/\text{sheet}$ and $5.0E+4 \Omega/\text{sheet}$ using this method.

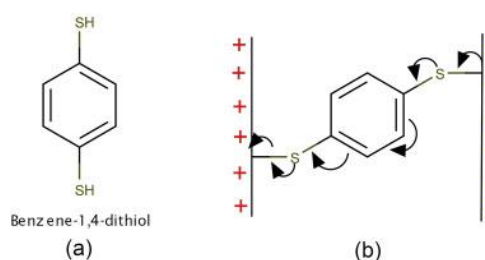


Fig. 4. (a) The molecular structure of benzene-1,4-dithiol and (b) a diagram of the chemical mechanism by which it would be expected to transfer charge between surfaces.

2.4. EIS testing for detectable surface interactions

To measure the binding interactions at the sensor surface the EIS spectrum from the surface over time was recorded when exposed to a molecule that would readily bind to it. For this test, the sensor was placed in a 3-electrode testing cell (see Fig. 5) containing 40 mL of PBS solution. When testing designs 1 and 2, measurements were performed using a glassy carbon counter electrode and silver chloride reference electrode whereas tests with design 3 made use of the built-in, screen printed counter/reference electrodes instead. An amount of 250 μL of 6-mercaptophexanol was then added to the solution and the surface was subjected to repeated EIS measurements on a loop over a specified time period. Each EIS measurement was performed spanning the 1–10,000 Hz range with a frequency resolution of 10 points per logarithmic decade. No DC voltage was applied and a root mean square AC voltage of 1 mV was applied during measurement. This resulted in an EIS spectrum plot of Z-phase vs time, allowing for the identification of changes in the electrochemical properties of the surface in response to the thiol added at time $t = 0$.

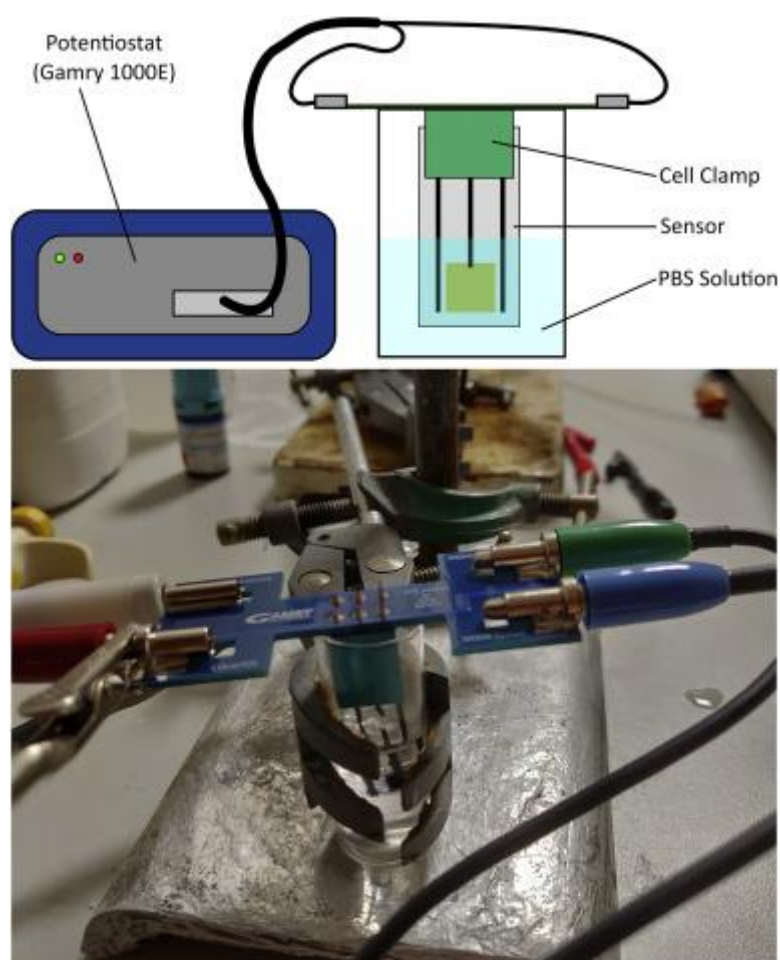


Fig. 5. A schematic (top) and photograph (bottom) of the testing cell setup used during EIS experiments with sensor design 3.

2.5. Chronoamperometric and cyclic voltammetry analyses

All chronoamperometry and cyclic voltammetry (CV) measurements were performed by placing the electrode in a 3-electrode testing cell containing 40 mL of PBS solution.

Chronoamperometry measurements were performed with a 0.5 s pre-step at 0 V, followed by a step to 0.5 V for 5 s and a step to 0.1 V for a final 5 s. CV measurements were obtained between a maximum and minimum voltage of 0.5 V and -0.5 V, at a scan rate of 10 mV/s across 10 cycles.

3. Results

3.1. Demonstration of measurable response to surface interactions

As described in Section 2.5, experiments were performed to measure the characteristics of these surfaces and track changes in these characteristics in response to a surface interaction. The data obtained from these tests were then plotted as response surfaces, as shown in Fig. 6. The level of the responses recorded can be used to evaluate the potential of this sensor fabrication method. All three designs that were developed showed a measurable and repeatable response for successive spectral acquisitions, however significantly larger signal responses were observed from designs 2 and 3.

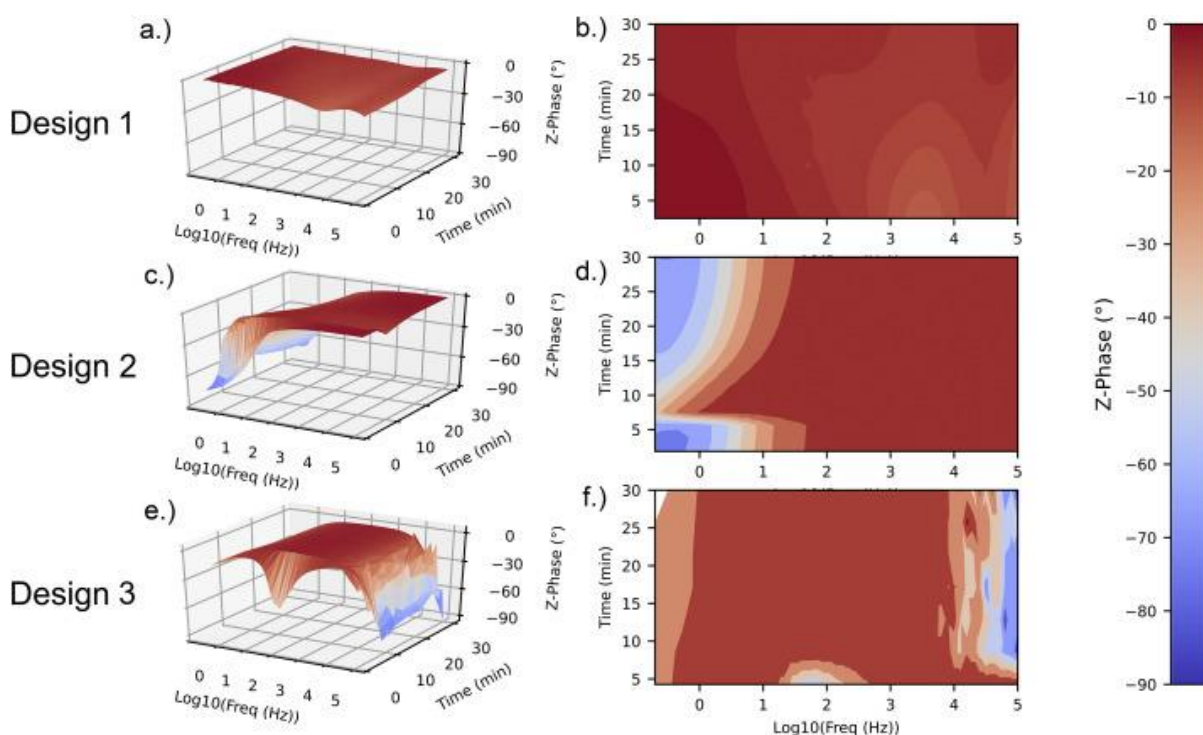


Fig. 6. Colour mapped plot showing the response surfaces for (a) design 1, (c) design 2, (e) design 3 and the contour plot for (b) design 1, (d) design 2, (f) design 3. In each test, 6-mercaptophexanol was added at $t = 0$.

The plots obtained during testing show a clear progression through the various examined stages of sensor development, at the stages of design 1, 2 and 3. The initial design tested (design 1) exhibited a slight response visible as a low intensity, a lingering peak between 1E3 Hz and 1E4 Hz, for which the phase angle gradually rose over the course of the hour long test. In response to this poor signal, screen printed contacts were added and the area of the sensing surface was increased for design 2.

Design 2 exhibited a significant increase in response, initially showing a peak at a phase angle below -80 degrees peaking at approximately a frequency of 1 Hz. This peak disappears within the first 10 min of testing, before gradually reappearing over the course of the experiment. In response to this significant signal, the area of the sensing surface was reduced for design 3.

Design 3, the final design, showed a clear peak present at 63 Hz that disappeared within the first 10 min following the introduction of a thiol to the solvent. Following this initial interaction, the phase at the 63 Hz frequency remains roughly constant showing no apparent evidence of any further measurable interactions.

3.2. Examination of the effects of crosslinking

The effects of the crosslinking step of the fabrication process were examined by recording chronoamperometry and cyclic voltammetry measurements before and after crosslinking (see Fig. 7).

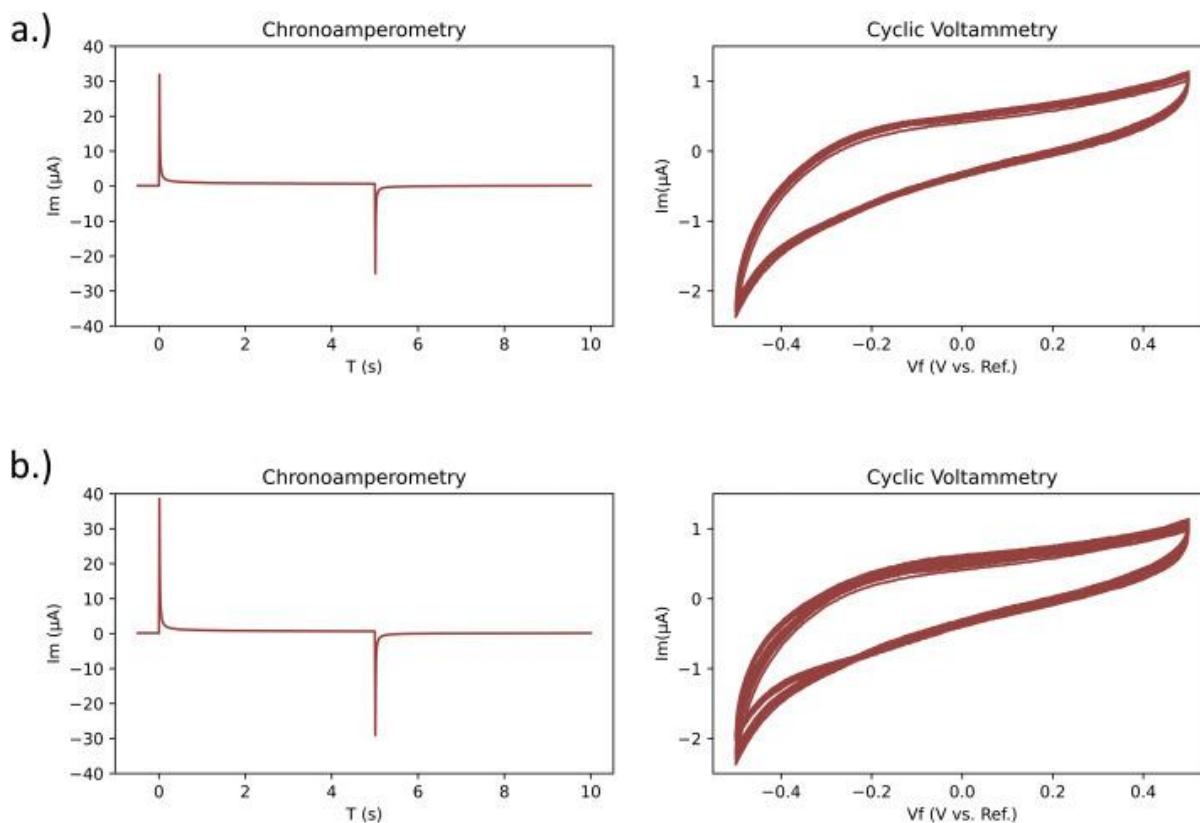


Fig. 7. Chronoamperometry and cyclic voltammetry plots obtained (a) before and (b) after the crosslinking step of the sensor fabrication process.

4. Discussion

The developed sensors show the potential of this fabrication method to produce a useful robust, sensitive and repeatable sensing surface. In this work, three different sensing areas and designs were developed and evaluated. The first, simple design tested (featuring a sensing surface and a simple CAP deposited line to a contact) showed no measurable response, due to breakages in the deposited surface. Despite numerous attempts to deposit the surface without breakages they were found to be unavoidable in the thin line section. Based on this failure, the deposited shape

was iteratively refined into the shape of the first successful sensor, design 1. Design 1 showed a small measurable response, representing an improvement over the earlier tested designs. During this test it was noted that unclamping and reclamping the contact would lead to changes in the observed EIS spectrum. Based on this, it was surmised that the poor response was likely due to this unreliable contact between the clamp and the nanostructured surface. It was also considered as a possibility that the resistivity of the contact track (the “neck” of the sensor as observable in Fig. 2) could be reducing the measurable signal.

To compensate for both of these hypothesised problems the next design (design 2) featured a screen printed contact and an increased 2d surface area of 10mm² was used. The addition of this conductive, screen printed contact was to ensure that contact with the clamp would be consistent and guarantee good conductance of signals from the sensing surface. This design showed a significant increase in observable change over time, resulting in the detection of a significant phase shift peak at the 1 Hz frequency, resulting from reaction to the introduction of the thiol at $t = 0$.

Due to the significant improvement of signal observed in design 2 the 2d surface area of the final sensor design (design 3) was reduced back to 25mm² to allow for the addition of counter and reference electrodes to the platform, allowing for its use in a standard three electrode cell setup. This design showed a clear phase shift peak at 100 Hz in the plot, irreversibly disappearing within 10 min of the introduction of a thiol.

A peak bode plot phase of -54.8 degrees was detected for design 3 at a frequency of 63.0 Hz after the first measurement ($t = 4.3$ min). Similarly, designs 1 and 2 showed their peak phase angles after the first measurement, at angles of -13.2 degrees at 3144 Hz ($t = 2.5$ min) and -75.5 degrees at 0.2 Hz ($t = 1.9$ min) respectively. Table 1 shows the peak responses and corresponding times and frequencies for each sensor design. It can be noted that the time required for each EIS measurement varied depending on the surface being tested.

Table 1. The peak data for each design at the time closest to the earliest measurement obtained using design 3.

Design number	Frequency (Hz)	Phase angle (degrees)	Time (min)
Design 1	3144	-12.5	5.0
Design 2	0.2	-75.6	3.8
Design 3	63.0	-54.8	4.3

Comparing the peak data visible in Table 1, it is clear that design 2 gave the largest response. However, a significant response was also present when testing design 3, a design which also had the additional benefit of incorporating reference and counter electrodes. Additionally, the response observed in design 2 was not four times the intensity of the response observed in design 3 despite its fourfold increased in area relative to design 3, demonstrating the higher efficiency of design 3 in terms of signal per unit area.

Once the electrode design was finalised, the effects of the crosslinking fabrication step were examined using chronoamperometry and cyclic voltammetry (CV). This data was then analysed to look for differences in electrode properties and to assess the stability of the resulting surface.

The chronoamperometry data obtained showed obvious differences in peak intensity before and after crosslinking was performed, with the peak maximum of 31.87 μA increasing to 38.58 μA (a 21.05% increase in instantaneous current), see Fig. 7. Similarly, the discharge peak minimum showed a decrease from $-24.96 \mu\text{A}$ to $-29.09 \mu\text{A}$ (a 17% increase in the intensity of this negative peak). In line with these measurements, the integral of the curve between the maximum of the charge peak and the beginning of the discharge peak also increased from 4.87 $\mu\text{A}\cdot\text{s}$ to 5.07 $\mu\text{A}\cdot\text{s}$. Based on the Cottrell equation, these increases in peak intensity and integrated area are most likely indicative of an increase in 3d surface area, as would be expected based on the crosslinking method used.

The CV data obtained before crosslinking showed no evidence of an anodic or cathodic peak, and this remained the case after the crosslinking step had been performed. This indicates that no significant redox reaction occurred within the voltage range examined, suggesting that the surfaces fabricated are likely to be stable following crosslinking. The average area enclosed by the CV plot before crosslinking was found to be 0.75 μW , with this area rising to 0.84 μW after crosslinking. Based on the Randles-Sevcik equation, this increase is most likely indicative of an increase in 3d surface area. This observation is therefore in agreement with the chronoamperometry data obtained.

5. Conclusions

The results obtained demonstrate the significant potential of the developed laser based fabrication methods as a tool for the production of nanostructured sensor surfaces. By applying these techniques the benefits of laser fabrication methods can be achieved for the application of nanotechnology to sensor production. By further optimising and automating the fabrication method, these surfaces could be mass produced at a low cost and high throughput, potentially expanding the accessibility of nanostructured sensor technology to a wider audience.

Surfaces produced using this method have also been demonstrated to exhibit a measurable, detectable response to surface interactions, a property that is vital for their use in a sensor platform. This response was demonstrated using repeated EIS measurements following the introduction of a thiol into solution, see Fig. 6. These tests showed clear peaks in the spectrum, generally disappearing within minutes following thiol introduction. The final sensor design, design 3, showed a clear phase angle of -54.8 degrees at a frequency of 63.0 Hz, disappearing completely within 10 min of the introduction of thiol. This demonstrates the disappearance of these peaks in response to a surface interaction.

Expanding upon this work, future work will include the examination of the scaleup of this process and the usage of these sensor surfaces in the detection of a biologically active target analyte.

Acknowledgements

This publication has emanated from research conducted with the financial support from Science Foundation Ireland (SFI) under Grant Number 12/IA/1576.

References

- [1] Y.-E. Choi, J.-W. Kwak, J.W. Park, Nanotechnology for early cancer detection *Sensors*, 10 (2010), pp. 428-455, 10.3390/s100100428
- [2] D. Grieshaber, R. MacKenzie, J. Vörös, E. Reimhult, Electrochemical biosensors - sensor principles and architectures, *Sensors*, 8 (2008), pp. 1400-1458 (2008;8:1400–58)
- [3] C. Paladiya, A. Kiani, Nano structured sensing surface: significance in sensor fabrication *Sensors Actuators B Chem.*, 268 (2018), pp. 494-511, 10.1016/j.snb.2018.04.085
- [4] J.K. Bhattarai, M.H. Uddin Maruf, K.J. Stine, Plasmonic-active nanostructured thin films *Processes*, 8 (2020), pp. 1-20, 10.3390/pr8010115
- [5] Y. Jiang, N. Liu, W. Guo, F. Xia, L. Jiang, Highly-efficient gating of solid-state nanochannels by DNA supersandwich structure containing ATP aptamers: a nanofluidic IMPLICATION logic device, *J. Am. Chem. Soc.*, 134 (2012), pp. 15395-15401, 10.1021/ja3053333
- [6] F. Xia, R.J. White, X. Zuo, A. Patterson, Y. Xiao, D. Kang, et al. An electrochemical supersandwich assay for sensitive and selective DNA detection in complex matrices *J. Am. Chem. Soc.*, 132 (2010), pp. 14346-14348, 10.1021/ja104998m
- [7] X. Jian, Y. Li, C. Zhao, Y. Chang, Z. Gao, Y.Y. Song, Introducing graphitic carbon nitride nanosheets as supersandwich-type assembly on porous electrode for ultrasensitive electrochemiluminescence immunosensing, *Anal. Chim. Acta*, 1097 (2020), pp. 62-70, 10.1016/j.aca.2019.10.070
- [8] J. Liu, M. Jalali, S. Mahshid, S. Wachsmann-Hogiu, Are plasmonic optical biosensors ready for use in point-of-need applications? *Analyst*, 145 (2020), pp. 364-384, 10.1039/c9an02149c
- [9] Z. Dai, J. Guo, J. Xu, C. Liu, Z. Gao, Y.Y. Song, Target-driven Nanozyme growth in TiO₂Nanochannels for improving selectivity in electrochemical biosensing, *Anal. Chem.*, 92 (2020), pp. 10033-10041, 10.1021/acs.analchem.0c01815
- [10] J. Guo, L. Yang, H. Xu, C. Zhao, Z. Dai, Z. Gao, et al., Biomineralization-driven ion gate in TiO₂ nanochannel arrays for cell H₂S sensing, *Anal. Chem.*, 91 (2019), pp. 13746-13751, 10.1021/acs.analchem.9b03119
- [11] N. Karimian, P. Ugo, Recent advances in sensing and biosensing with arrays of nanoelectrodes *Curr Opin Electrochem*, 16 (2019), pp. 106-116, 10.1016/j.coelec.2019.04.026
- [12] M.H. Seo, J.Y. Yoo, M.S. Jo, J.B. Yoon Geometrically structured nanomaterials for nanosensors, NEMS, and nanosieves *Adv. Mater.*, 1907082 (2020), pp. 1-24, 10.1002/adma.201907082

- [13] M.G. Stanford, P.D. Rack, D. Jariwala, Emerging nanofabrication and quantum confinement techniques for 2D materials beyond graphene, *Npj 2D Mater Appl*, 2 (2018), 10.1038/s41699-018-0065-3
- [14] D. Zhang, B. Gökce, S. Barcikowski, Laser synthesis and processing of colloids: fundamentals and applications, *Chem. Rev.*, 117 (2017), pp. 3990-4103, 10.1021/acs.chemrev.6b00468
- [15] S. Besner, A.V. Kabashin, F.M. Winnik, M. Meunier, Ultrafast laser based “green” synthesis of non-toxic nanoparticles in aqueous solutions, *Appl. Phys. A Mater. Sci. Process.*, 93 (2008), pp. 955-959, 10.1007/s00339-008-4773-y
- [16] R. Kumar, G. Kumar, A. Umar, Pulsed laser deposited nanostructured ZnO thin films; a review, *J. Nanosci. Nanotechnol.*, 14 (2014), pp. 1911-1930, 10.1166/jnn.2014.9120
- [17] V. Serbezov, Pulsed laser deposition: the road to hybrid Nanocomposites coatings and novel pulsed laser adaptive technique, *Recent Pat Nanotechnol*, 7 (2012), pp. 26-40, 10.2174/18722105130104
- [18] F.J. Adrian, J. Bohandy, B.F. Kim, A.N. Jette, P. Thompson, A study of the mechanism of metal deposition by the laser-induced forward transfer process, *J Vac Sci Technol B*, 5 (1987), pp. 1490-1494, 10.1116/1.583661
- [19] A. Piqué, H. Kim, R.C.Y. Auyeung, I. Beniam, E. Breckenfeld, Laser-induced forward transfer (LIFT) of congruent voxels, *Appl. Surf. Sci.*, 374 (2016), pp. 42-48, 10.1016/j.apsusc.2015.09.005
- [20] G. Dhimi, B. Tan, K. Venketakrishnan, Laser induced reverse transfer of gold thin film using femtosecond laser, *Opt. Lasers Eng.*, 49 (2011), pp. 866-869, 10.1016/j.optlaseng.2011.02.019
- [21] C. Hughes, R. McCann, J. Eguileor, K. Bagga, R. Groarke, F. Regan, et al. Modelling and optimisation of single-step laser-based gold nanostructure deposition with tunable optical properties *Opt. Laser Technol.*, 108 (2018), pp. 295-305, 10.1016/j.optlastec.2018.06.063
- [22] R. McCann, C. Hughes, K. Bagga, A. Stalcup, M. Vázquez, D. Brabazon, Pulsed laser deposition of plasmonic nanostructured gold on flexible transparent polymers at atmospheric pressure, *J. Phys. D. Appl. Phys.*, 50 (2017), p. 245303
- [23] K. Bagga, R. McCann, M. Wang, A. Stalcup, M. Vázquez, D. Brabazon, Laser assisted synthesis of carbon nanoparticles with controlled viscosities for printing applications, *J. Colloid Interface Sci.*, 447 (2015), pp. 263-268, 10.1016/j.jcis.2014.10.046
- [24] S. Reich, P. Schönfeld, P. Wagener, A. Letzel, S. Ibrahimkutty, B. Gökce, et al. Pulsed laser ablation in liquids: impact of the bubble dynamics on particle formation, *J. Colloid Interface Sci.*, 489 (2017), pp. 106-113, 10.1016/j.jcis.2016.08.030
- [25] Y. Ishikawa, N. Koshizaki, A. Pyatenko, Submicrometer-sized spherical Iron oxide particles fabricated by pulsed laser melting in liquid, *Electron Commun Japan*, 99 (2016), pp. 37-42, 10.1002/ecj.11898

[26] M. Kondo, N. Shishido, S. Kamiya, A. Kubo, Y. Umeno, Y. Ishikawa, et al. High-strength sub-micrometer spherical particles fabricated by pulsed laser melting in liquid Part. Part. Syst. Charact., 35 (2018), pp. 1-9, 10.1002/ppsc.201800061

[27] L.A. Dobrzański, A.D. Dobrzańska-Danikiewicz, Applications of laser processing of materials in surface engineering in the industry 4.0 stage of the industrial revolution, Mater Perform Charact., 8 (2019), p. 20190203, 10.1520/MPC20190203

[28] B. Freeland, R. McCann, G. Alkan, B. Friedrich, G. Foley, D. Brabazon, Stable nano-silver colloid production via laser ablation synthesis in solution (LASiS) under laminar recirculatory flow, Adv Mater Process Technol., 00 (2020), pp. 1-9, 10.1080/2374068X.2020.1740877,

[29] Y. Jin, K.H. Wong, A.M. Granville, Developing localized surface plasmon resonance biosensor chips and fiber optics via direct surface modification of PMMA optical waveguides, Colloids Surfaces A Physicochem Eng Asp, 492 (2016), pp. 100-109, 10.1016/j.colsurfa.2015.11.025